Evolution of High-energy Particle Distribution in Supernova Remnants

Houdun Zeng , Yuliang Xin, and Siming Liu

Purple Mountain Observatory, Chinese Academy of Sciences. liusm@pmo.ac.cn and zhd@pmo.ac.cn

Abstract

In this paper, we fit the spectral energy distributions of 35 SNRs with a simple one-zone emission model and analyze correlations of model parameters to uncover the evolution of high-energy particle distribution in SNRs. We find that **(1)** the particle distribution in general can be described by a broken power-law function with a high-energy cutoff for all SNRs; **(2)** the low-energy spectrum becomes harder and the break energy decreases with aging of SNRs, **(3)** for most middle-age SNRs, the energy loss timescale of electrons at the high-energy cutoff is approximately equal to the age of the corresponding remnant implying quenching of very-high-energy electron acceleration; for young SNRs, this energy loss timescale is shorter than the age of SNRs implying continuous electron acceleration at the cutoff energy; and for a few old age SNRs, the energy loss timescale is longer than the corresponding age, which may suggest escaping of higher energy particles from SNRs. **Finally**, we comment on the implications of these results on the SNR origin of Galactic cosmic rays.

Sample

We use their latest database [a], which summarizes the basic physical properties and observational status of all SNRs (Green 2017), and find 35 SNRs with both radio and GeV spectra. Complex SNRs, such as Cas A, are not considered because their emission is not consistent with a simple one-zone emission model. Among these 35 sources, 6 are detected with nonthermal X-ray emission and 16 have TeV spectral measurements.

[a] http://www.physics.umanitoba.ca/snr/SNRcat/

Models

We consider a simple one-zone emission model with high-energy particle distributions given by

$$N(P_i) = N_{0,i}e^{(-\frac{P_i}{P_{i,cut}})}\begin{cases} P_i^{-\alpha} & \text{if} P_i < P_{\rm br} \\ P_{i,\rm br}P_i^{-(\alpha+1)} & \text{if} P_i \geq P_{\rm br} \end{cases}$$

which "i" represents different particle species, $P_{\rm e,cut} < P_{\rm p,cut}$ are the high-energy cutoffs of electron and proton distributions, respectively, and we have assumed an identical spectral break for electron and protons. Considering the SNR origin of Galactic cosmic rays, $N_{0,e}/N_{0,p}$ is fixed at 0.01. Our model contain leptonic (Brem and IC) and hadronic (π^0 decay) γ-ray emission processes. For cases where $P_{e,cut}$ is poorly constrained, we fix $P_{e,cut}$ by requiring the radiative energy loss timescale being equal to the age of the corresponding SNR. Then there will be five free parameters.
We use the Markov Chain Monte Carlo (MCMC) algorithm to carry out the spectral fit.

References

[1] Green, D. A. 2017, A Catalogue of Galactic Supernova Remnants (Cambridge: Cavendish Laboratory), http://www.mrao.cam.ac.uk/surveys/snrs/

[2] Zeng, H., Xin, Y., Liu, S., et al. 2017, ApJ, 834, 153

[3] **Zeng, H., Xin, Y. and Liu, S. 2019, ApJ, 874, 50**

SED of 35 SNRs

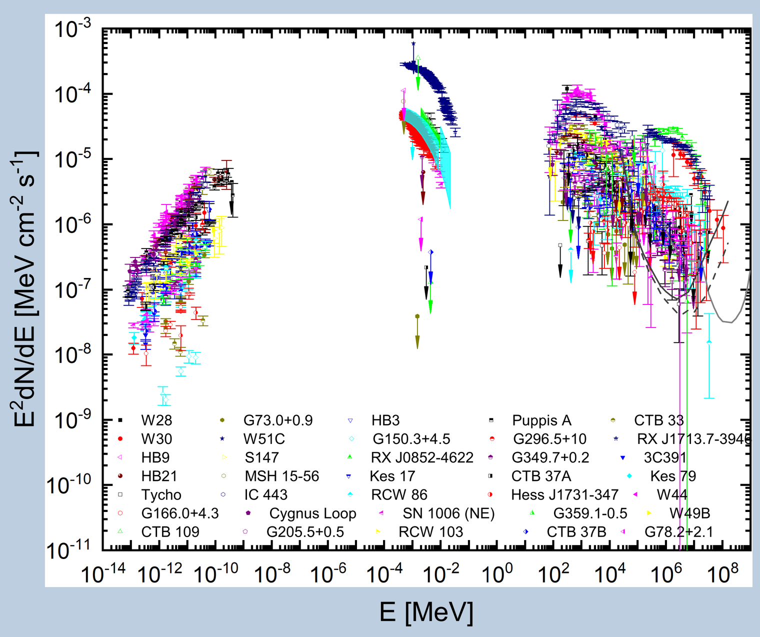

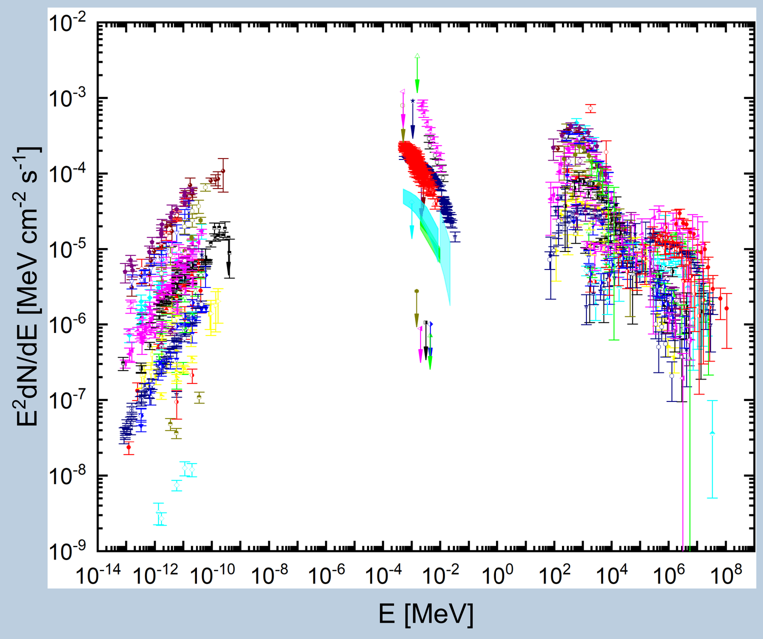

The Sample of SNRs and Related Physical Information

SNR Name	Other Name	Radius (pc)	Distance (Kpc)	Age (kyr)	Density (cm^{-3})	Shock Speed (km s^{-1})
G006.4−00.1	W28	~13	~2.0	40(33–150)	~100	60–80
G008.7−00.1	W30	~26	~4.0	25(15–28)	~100	530–750
G031.9+00.0	3C 391	~7	~7.2	~4	~300	620–730
G033.6+00.1	Kes 79	~9.6	~7.0	~4.4–6.7	~3(1–5)	400 ± 5
G034.7−00.4	W44	~12.5	~3.0	~20	~200	100–150
G043.3−00.2	W49B	~5	~10	~5.7(5–6)	~700	~400
G049.2−00.7	W51C	~18	~4.3	~30	~10	~100
G073.9+00.9		~16/5.2	~4.0/1.3	~11–12	~10	~200–300
G074.0−08.5	Cygnus loop	~16	~0.54	~14	~5.0	240–330
G078.2+02.1	γ Cygni	~17	~2.0	~8.25(6.8–10)	~2.5(0.1–20)	700–1100
G089.0+04.7	HB21	~26	~1.7	~4.8(3.6 or 45)	~15	~125
G109.1−1.00	CTB109	~16	~3.1	~9.0(9.0–9.2)	~1.1	~230 ± 5
G120.1+01.4	Tycho	~3.3	~3.0	~0.44	~10/0.3	4600–4800
G132.7+01.3	HB3	~26.4	~2.2	~30.0	~2.0	303–377
G150.3+04.5		~9.4	~0.40	~1.5(0.5–5)	~1.0	<2500
G160.9+02.6	HB9	~15	~0.8	5.3(4–7)	~0.1	~740
G166.0+04.3		~26	~4.5	24.0	~0.01	~680
G180.0−01.7	S147	~38	~1.3	30(20–100)	~250(100–500)	~500
G189.1+03.0	IC 443	~11	~1.5	~30	~140	60–100
G205.5+0.50	Monoceros	~63.36	~1.98	~30	~3.6	~50
G260.4−03.4	Puppis A	~15	~2.2	4.45(3.75–5.20)	~4.0	700–2500
G266.2−01.2	RX J0852–4622	~13	~0.75	2.7(1.7–4.3)	~3.8	~3000
G296.5+10.0		~26	~2.1	~10.0	~13.0	<1000
G304.6+00.1	Kes 17	~10	~10	4.2(2–5.2)	~10	150–200
G315.4−02.3	RCW 86	~15	~2.5	~1.8	~0.1–2.0	700–2000
G326.3−01.8	MSH 15–56	~22.2	~4.1	~10.0(10–16.5)	~0.1/1.0	500–860
G327.6+14.6	SN 1006	~9.0	~2.2	~1.0	~0.085	3200–5800
G332.4−00.4	RCW 103	~5	~3.3	~2.0	~10	~1100
G337.0−00.1	CTB 33	~2.55	~11.0	~5.0	~60	<200
G347.3−00.5	RX 1713.7–3946	~10	~1.0	~1.6	~0.01	~5000
G348.5+00.1	CTB 37A	~10	~7.9	~30	~100	75–100
G348.7+00.3	CTB 37B	~20	~13.2	~5	~10/0.5	~800

The left panel shows the multi-wavelength spectral data of 35 SNRs. The middel panel shows the spectra normalized at 100 GeV to 10^{-5} MeV cm^{-2} s^{-1}. The right panel shows the radius, distance, age, medium density, shock velocity of some sources.

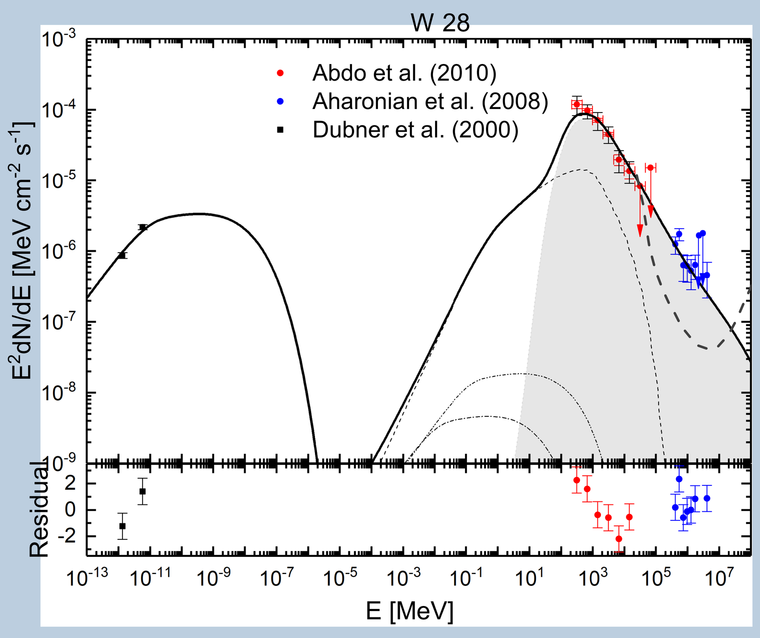

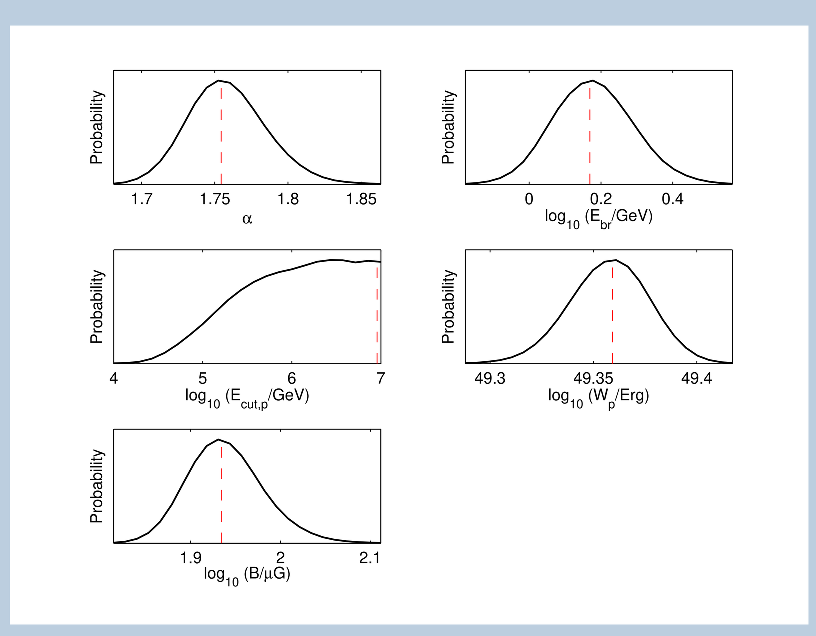

Spectral Fitting Parameters

Source Name	α	$\log_{10}\frac{E_{\rm br}}{\rm GeV}$	$\log_{10}\frac{E_{\rm e,cut}}{\rm GeV}$	$\log_{10}\frac{E_{\rm p,cut}}{\rm GeV}$	$\log_{10}\frac{B}{\mu\rm G}$	$\log_{10}\frac{W_p}{\rm erg}$	$\frac{W_B}{W_e}$	$\frac{n}{\rm cm^{-3}}$	$\frac{\chi^2}{\rm NDF}$
W28	$1.76^{+0.03}_{-0.03}$	$0.18^{+0.11}_{-0.11}$	1.63	>5.72	$1.94^{+0.04}_{-0.04}$	$49.36^{+0.02}_{-0.02}$	3000	100	$\frac{24.3}{10}=2.43$
W30	$1.63^{+0.10}_{-0.11}$	$0.24^{+0.33}_{-0.38}$	2.06	>4.29	$1.86^{+0.12}_{-0.13}$	$49.69^{+0.07}_{-0.07}$	736	100	$\frac{6.0}{7}=0.86$
3C391	$1.99^{+0.05}_{-0.05}$	$1.15^{+0.14}_{-0.14}$	1.86	>3.81	$2.31^{+0.04}_{-0.04}$	$49.03^{+0.03}_{-0.03}$	619	300	$\frac{37.1}{19}=1.95$
Kes79[c]	$2.00^{+0.08}_{-0.08}$	NA	$E_{\rm p,cut}$	$1.07^{+0.16}_{-0.16}$	$1.70^{+0.05}_{-0.05}$	$49.47^{+0.04}_{-0.04}$	21.3	100.0	$\frac{64.2}{24}=2.68$
W44	$1.60^{+0.04}_{-0.04}$	$0.73^{+0.09}_{-0.09}$	1.23	$1.87^{+0.11}_{-0.09}$	$2.28^{+0.03}_{-0.03}$	$49.43^{+0.01}_{-0.01}$	1480	200	$\frac{44.4}{48}=0.93$
W49B	$1.47^{+0.04}_{-0.04}$	$-0.21^{+0.23}_{-0.24}$	1.55	$3.70^{+0.13}_{-0.13}$	$2.40^{+0.06}_{-0.06}$	$49.43^{+0.02}_{-0.02}$	235	700	$\frac{18.9}{20}=1.00$
W51C	$1.56^{+0.02}_{-0.02}$	$0.31^{+0.08}_{-0.08}$	1.64	$4.39^{+0.30}_{-0.29}$	$2.08^{+0.03}_{-0.03}$	$49.83^{+0.01}_{-0.01}$	708	100	$\frac{59.7}{29}=2.06$
W51C[b]	$1.64^{+0.02}_{-0.02}$	$0.32^{+0.05}_{-0.05}$	1.57	>5.78	$2.02^{+0.03}_{-0.03}$	$49.79^{+0.01}_{-0.01}$	201	100	$\frac{34.9}{29}=1.20$
G73.9+0.9[c]	$0.78^{+0.19}_{-0.19}$	NA	$E_{\rm p,cut}$	$0.96^{+0.09}_{-0.09}$	$1.57^{+0.05}_{-0.05}$	$49.34^{+0.04}_{-0.04}$	393	10	$\frac{22.4}{13}=1.72$
Cygnus Loop[c]	$1.86^{+0.08}_{-0.08}$	NA	$E_{\rm p,cut}$	$1.09^{+0.10}_{-0.10}$	$1.46^{+0.03}_{-0.03}$	$48.72^{+0.02}_{-0.02}$	197	5.0	$\frac{20.5}{20}=1.03$
γ Cygni	$2.00^{+0.05}_{-0.05}$	$3.17^{+0.17}_{-0.18}$	2.63	>4.97	$1.78^{+0.05}_{-0.05}$	$50.25^{+0.02}_{-0.02}$	61.5	2.5	$\frac{23.6}{18}=1.31$
HB21[c]	$1.20^{+0.12}_{-0.12}$	NA	$E_{\rm p,cut}$	$0.69^{+0.04}_{-0.05}$	$1.71^{+0.01}_{-0.01}$	$49.42^{+0.01}_{-0.01}$	564	15	$\frac{36.2}{23}=1.57$
CTB109	$1.94^{+0.09}_{-0.09}$	$2.66^{+0.38}_{-0.81}$	3.28	>4.82	$1.47^{+0.17}_{-0.20}$	$49.84^{+0.12}_{-0.12}$	19.6	1.1	$\frac{20.9}{8}=2.61$
Tycho	$2.15^{+0.02}_{-0.02}$	$3.37^{+0.12}_{-0.12}$	$4.14^{+0.08}_{-0.09}$	>5.04	$2.15^{+0.04}_{-0.05}$	$49.01^{+0.08}_{-0.08}$	23.5	0.3	$\frac{55}{35}=1.57$
Tycho	$2.16^{+0.02}_{-0.02}$	$3.36^{+0.11}_{-0.11}$	$4.06^{+0.07}_{-0.07}$	>4.93	$2.29^{+0.04}_{-0.05}$	$48.78^{+0.07}_{-0.07}$	92.2	10.0	$\frac{44}{35}=1.26$
HB3[c]	$1.84^{+0.17}_{-0.16}$	NA	$E_{\rm p,cut}$	$1.08^{+0.17}_{-0.17}$	$1.04^{+0.04}_{-0.04}$	$50.04^{+0.03}_{-0.03}$	6.4	2.0	$\frac{16.4}{19}=0.86$
G150.3+4.5	$1.73^{+0.22}_{-0.22}$	$2.65^{+0.36}_{-0.42}$	6.04	>6.37	$0.45^{+0.13}_{-0.13}$	$48.33^{+0.05}_{-0.05}$	1.42	1.0	$\frac{11.5}{12}=0.96$
HB9[c]	$1.75^{+0.32}_{-0.34}$	NA	$E_{\rm p,cut}$	$1.11^{+0.43}_{-0.40}$	$0.61^{+0.07}_{-0.08}$	$50.25^{+0.08}_{-0.08}$	0.07	0.1	$\frac{7.3}{12}=0.61$
G166.0+4.3[c]	$1.32^{+0.17}_{-0.18}$	NA	$E_{\rm p,cut}$	$1.87^{+0.14}_{-0.15}$	$0.57^{+0.24}_{-0.24}$	$50.92^{+0.26}_{-0.25}$	0.12	0.01	$\frac{6.92}{5}=1.38$
G166.0+4.3[c]	$1.26^{+0.17}_{-0.18}$	NA	$E_{\rm p,cut}$	$1.18^{+0.16}_{-0.16}$	$1.62^{+0.10}_{-0.10}$	$49.18^{+0.07}_{-0.07}$	717	10.0	$\frac{7.70}{5}=1.54$
S147	$1.36^{+0.06}$[illegible]	$-0.14^{+0.12}$[illegible]	0.09	>3.86	$2.77^{+0.09}$[illegible]	$47.71^{+0.05}$[illegible]	2.7×10^{8}	250	$\frac{17.3}{[illegible]}=1.02$
IC 443	[illegible]	[illegible]	[illegible]	[illegible]	[illegible]	[illegible]	[illegible]	[illegible]	[illegible]

Example: the best fit to the SED and 1D probability distribution of the parameters for W28. The right table lists the model parameters, α, E_{br}, $E_{e,cut}$, $E_{p,cut}$, the magnetic field for synchrotron emission, B, and the total energy content of protons, W_p, with $E > 1$ GeV for a given density and distance, as well as the ratio W_B/W_e, the adopted density, and the reduced χ^2 for the best-fit of part SNRs.

Analyze correlations of model parameters

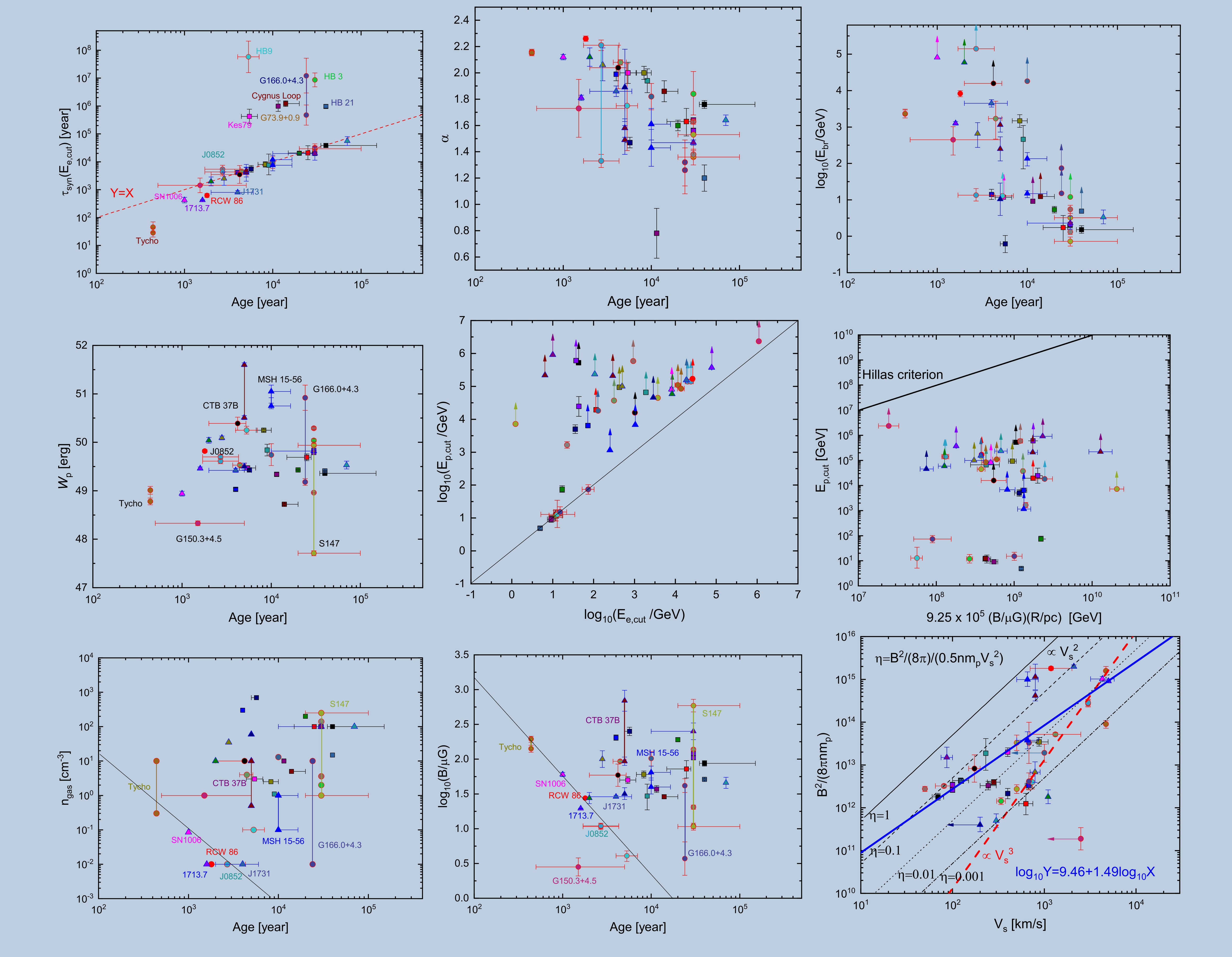

Multiwavelength observations of SNRs provide a unique opportunity to study evolution of high-energy particle distribution trapped with SNRs, which is closely related to the particle acceleration and escape processes. In this paper, we extend our earlier comparative spectral study of three SNRs to a sample of 35 SNRs (Zeng et al. 2017). In general, our results are compatible to the scenario of SNR origin of Galactic cosmic rays. Young SNRs have relatively soft spectra; however, their break energies are high so that they may dominate the flux of high-energy cosmic rays. Although the low-energy spectra of old SNRs are hard, their break energies are low. They likely dominate fluxes of cosmic rays with relatively lower energies